Morphological development of rip channel systems: Normal and near-normal wave incidence

D. Calvete,[1] N. Dodd,[2] A. Falqués,[1] and S. M. van Leeuwen[2]

[1] The process of formation of a rip channel/crescentic bar system on a straight, sandy coast is examined. A short review of earlier studies is presented. A morphodynamic stability model is then formulated. The resulting model includes a comprehensive treatment of shoaling and surf zone hydrodynamics, including wave refraction on depth and currents and waves. The sediment transport is modeled using a total load formula. This model is used to study the formation of rip currents and channels on a straight single-barred coast. It is found that this more comprehensive treatment of the dynamics reveals the basic rip cells predicted in earlier studies for normal incidence. Also as before, cell spacings (λ) scale with shore-to-bar crest distance (X_b), while growth rates decrease. The λ increases with offshore wave height (H) up to a saturation value; increasing H also increases instability. Experiments at off-normal wave incidence ($\theta > 0$) introduce obliquity into the evolving bed forms, as expected, and λ increases approximately linearly. the e-folding times also increase with θ. At normal incidence, λ increases weakly with wave period, but at oblique angles, λ decreases. Tests also reveal the presence of forced circulation cells nearer to the shoreline, which carve out bed forms there. The dynamics of these forced cells is illustrated and discussed along with the associated shoreline perturbation. Transverse bars are also discovered. Their dynamics are discussed. Model predictions are also compared with field observations. The relevance of the present approach to predictions of fully developed beach states is also discussed.

1. Introduction

[2] It is common knowledge that the nearshore region (shoaling, surf and swash zones) is highly complex, where wave energy is transformed and dissipated. One characteristic of this region is the frequent formation of sometimes complex horizontal wave-driven circulation patterns, and the linked development of a beach profile with various bed forms and bars. Along a straight, sandy coast it is common for at least one alongshore, shore-parallel bar to develop, on which much of the wave breaking occurs. When a bar is present it is also common to see rip currents, which are strong (up to $\sim$2 m s^{-1}) offshore flowing currents. These currents form part of the larger circulation system, and carry offshore water driven onshore over a wider stretch of shore by wave breaking and set-up. They occur together with a morphological pattern consisting of shallower and deeper areas alternating along the bar. The rip currents are concentrated at the deeper bar sections: the rip channels. The shallower sections are typically located onshore of the mean bar crest while the deeper areas are offshore of it so that the overall shape of the bar in plain view consists of crescents, the horns being shallower and facing the shore. The whole morphological pattern is referred to as a crescentic bar. It is a remarkable fact that these currents and morphological patterns can occur in apparently organized systems, in which the spacing between rip channels is a quasi-regular length. When wave incidence is predominantly at an oblique angle, quasi-rhythmic circulation currents and channels can also exist, but it is at approximately normal incidence that this alongshore rhythmic feature is usually at its most startling.

1.1. Literature Review

[3] In Table 1 of *van Enckevort et al.* [2004], up to 33 references on crescentic bar observations are listed worldwide, dating back to 1949. Crescentic bars are characteristic of intermediate beaches [*Wright and Short*, 1984; *Lippmann and Holman*, 1990] and are commonly wiped out during storms, but form again after the peak of the storm. This behavior has been systematically observed, for instance, at Duck (North Carolina, Atlantic USA coast), at

---

[1]Departament de Física Aplicada, Universitat Politécnica de Catalunya, Barcelona, Spain.
[2]School of Civil Engineering, University of Nottingham, Nottingham, UK.

Miyazaki (Kyushu, Japan) and at Gold Coast (Queensland, Australia) by *van Enckevort et al.* [2004]. The destruction typically occurs for $\Omega = H_b/T w_s \sim 7-10$ or higher, where H_b is wave height at breaking, T wave period and w_s sediment fall velocity. The formation time is about $1-3$ days. Wavelength, λ, defined as the distance between consecutive rip channels, ranges from several tens of meters to two or three kilometers and it increases with the distance from the shoreline to the bar crest, X_b. Values of λ/X_b reported in the literature are in the order $1-10$. For instance, values observed at Duck and at Miyazaki by *van Enckevort et al.* [2004] during the initial formation of the rip channels were about $7-10$. Afterward, spacing tended to decrease, that ratio becoming about $2-6$. Values reported by *Castelle* [2004] from the Aquitaine coast (southern French Atlantic coast) range between 1 and 4.

[4] The origin of crescentic bars had been attributed to infragravity edge wave forcing, the morphology responding passively to the hydrodynamics [*Bowen and Inman*, 1971; *Holman and Bowen*, 1982]. In recent years, however, several studies have shown that crescentic bars can be generated just by a morphodynamic instability of the linear shore-parallel bar owing to a positive feedback between the developing topography and the flow. *Deigaard et al.* [1999] were the first to examine such an instability for a barred beach profile [see also *Hino*, 1974; *Christensen et al.*, 1994; *Falqués et al.*, 1996]. Unusually, they used of a fully nonlinear finite difference model to perform a linear stability analysis, and obtained growing topographic patterns with an *e*-folding time of about 12 hours. Their rip channel spacings were about 10 X_b for oblique wave incidence, and $8-10$ times the distance to the outer breaker zone. Significantly, this was less ($\sim 2.5\ X_b$) for normal incidence. The lengthscale of the emerging bed forms was strongly dependent on X_b, and in fact $\lambda \propto \sqrt{\text{trough area}}$. Evolving bed forms appeared virtually symmetric in the alongshore coordinate. In contrast, the current perturbation shows a clear anti-symmetry compared with normal incidence.

[5] *Falqués et al.* [2000] pursued an idealized approach in order to isolate the "bed-surf" coupling. They considered normal wave incidence and a plane beach (and regular waves), and imposed a saturated surf zone. Their evolving crescentic patterns consist of a double row of shoals and channels alternating at both sides of the breaker line, with channels shoreward of the breakpoint carrying offshore flowing current onto the shoals just offshore, and vice versa. The $\lambda \sim 3-4$ times the surf zone width and is related to the efficiency of the circulation cells. They also identified the importance of the ratio between the wave stirring coefficient (α, proportionality coefficient between sediment flux and current, representing the tendency of the waves to mobilize sediment) to the depth (D) as the main criterion for morphodynamic (in)stability. Thus an undulation on top of the bar produces onshore current over the shallower parts and offshore current over the deeper parts. This is because a bump (channel) induces a slightly increased (decreased) gradient in radiation stress [see also *Deigaard et al.*, 1999]). Then if α increases seaward of the bar crest, onshore current will take more sediment from the break point into the bar than it removes from the bar crest to the trough (and the opposite for offshore current). This effect competes with

flow acceleration due to continuity, hence the importance of the ratio α/D (called "potential stirring"). If potential stirring increases offshore toward the break point wave stirring dominates over mass conservation and the perturbation will grow.

[6] The mechanism was also found to work in the finite amplitude regime by *Caballeria et al.* [2002]. Their study, using a finite difference model, included wave refraction on the developing bed forms, and this led to the formation of shore-transverse bars, sometimes competing and sometimes coexisting with the crescentic patterns in a complex dynamics. *Coco et al.* [2003] extended this work to a barred beach profile, and used a realistic potential stirring profile. It was found that the growing crescentic pattern shaped the bar, the inner shoals corresponding to the shore facing horns, the inner troughs to rip channels and the outer shoals to deltas seaward of the rip channels.

[7] *Damgaard et al.* [2002] examine a barred beach at normal incidence for random waves, comparing predictions from a linear stability analysis with results of simulations using a fully nonlinear commercial finite difference code. Starting from an alongshore uniform situation (either as the basic state for the stability analysis or as a starting point for the numerical simulation) both approaches predict the formation of rip channels, with $1.4 X_b < \lambda < 5.6\ X_b$, and both sets of results clustered between 2 and 4 X_b. The initial growth rates predicted by the fully nonlinear code are remarkably similar to those rates predicted by the linear stability model.

[8] The linear stability approach to investigate the formation of rip channel has also been pursued in case of both a single- and a double-barred beach has been considered by *Klein et al.* [2003], who follow an approach similar to *Deigaard et al.* [1999], in computing the morphodynamic eigenvalues by iteration from fully nonlinear flow simulations. They also examine oblique wave incidence. Their results were largely in line with those of *Deigaard et al.* [1999], although their *e*-folding times were very large (~ 800 hours).

[9] Most recently, a more sophisticated (nonlinear) model was used by *Reniers et al.* [2004] to look at the complicated dynamics on an embayed barred beach. Essentially the model is similar to that used by *Damgaard et al.* [2002], but includes a parametric description of undertow. The most relevant difference is, however, that it allows for low frequency forcing by wave groups and directional spreading in the incident waves. Thus the model is capable of describing infragravity edge waves and their interaction with the morphodynamics. This is important since infragravity edge waves have been actually measured at some beaches where crescentic bars were present [e.g., *Aagaard*, 1991], giving support to the edge wave hypothesis. Moreover, *Vittori et al.* [1999] have shown that a crescentic pattern and an edge wave can grow at the same time, coupled with each other in a positive feedback. However, *Reniers et al.* [2004] obtained similar results to *Damgaard et al.* [2002] and *Coco et al.* [2003] and concluded that, at least in some conditions, the crescentic shape is essentially due to morphodynamic self-organization, the edge waves being just the result of the morphology and not the other way around (they filtered out edge waves from their simulations and repeated their tests). They found, however,
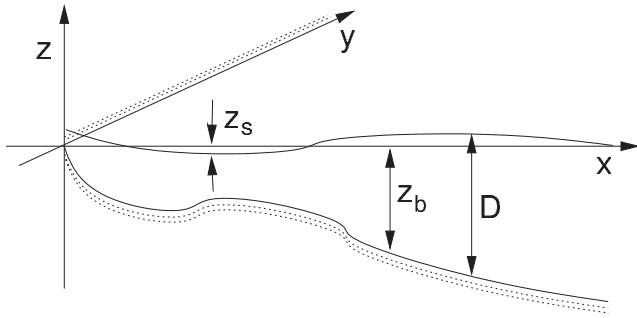
Figure 1. Coordinate system.

a significant influence of the directional spreading on the alongshore spacing which is in the range $1–2.5\ X_b$.

1.2. Present Study

[10] The self-organized origin of crescentic bars through bed-surf coupling seems now well established by both linear stability analyses and stability tests with fully nonlinear models. There are, however, several aspects that require further attention. First, there are substantial differences between formation times predicted by the models, ranging from about 0.5 up to 30 days, whereas observations of *van Enckevort et al.* [2004] suggest $1–3$ days. An exception are the bars on the Dutch coast, which have a considerably longer time scale. This is hypothesized to a consequence of their large size. Second, while the width of the surf zone sets the basic lengthscale for rhythmic features along an un-barred coast, several other lengths such as X_b, depth at the crest and depth at the trough can play a role for a barred beach [*Calvete et al.*, 2003; *Caballeria et al.*, 2003]. Therefore predicting λ on a barred beach can be more difficult. The aforementioned studies give the range and suggest some trends, but a systematic study is lacking. In particular, while initial spacings observed by *van Enckevort et al.* [2004] at several beaches are about $7–10\ X_b$, existing models give a substantially smaller $\lambda \sim 1–5.5\ X_b$, for normal wave incidence, and about $10\ X_b$ for oblique incidence. Thus normal incidence seems essentially different from oblique incidence, an observation borne out by *Deigaard et al.* [1999] [see also *Ribas et al.*, 2003]. Furthermore, waves are rarely exactly normally incident, so examining, as we do here, the difference between exact and almost normal incidence is desirable. In examining this regime we may tentatively assess the effect of wave spreading, although this is beyond the scope of the present study. Lastly, all linear stability studies presented so far have possessed substantial limitations (aside from that of linearity and periodicity), apart from that of *Calvete et al.* [2003], who presented a stability model based on a perturbation analysis of the full equations of nearshore dynamics without further approximation. We extend this study significantly, presenting the full equations, and performing a more thorough and comprehensive analysis.

[11] Here, therefore, we present a linear stability analysis of a straight, barred beach. This approach, based on the assumption of alongshore spatial periodicity, is ideally suited to examining rhythmic topography on a straight coast [see *Dodd et al.*, 2003], and allows us to isolate

physical mechanisms efficiently, without the added complication of numerical instabilities and diffusion. Even though the actual spacing in nature may be dictated by the finite amplitude dynamics, the present approach is more efficient in investigating parametric trends for the spacing. The comprehensive approach taken allows us to include wave refraction by the developing topography and by currents.

[12] In the next section we present the stability model (basic state and perturbation). Thereafter we look in detail at crescentic bar development on a barred beach. We conduct a comprehensive parametric study, examining wave height, period, angle of incidence and sediment properties, and look at the effect of bar position. We postpone detailed discussion of results until the following section. There we discuss physical mechanisms, the different types of bed forms observed (not just crescentic bars), and compare with previous studies. Finally, conclusions are presented.

2. Model Description

2.1. Equations of Motion

[13] The coordinate system is depicted in Figure 1, which shows an alongshore-uniform coast (x/x_1 the cross-shore, and y/x_2 the alongshore direction). We consider the depth- and time-averaged equations of continuity (1a) and momentum (1b), and therefore depth-uniform currents, along with a wave energy (1c) and phase (1d) equations, and a sediment conservation equation (1e). The resulting system is

$$\frac{\partial D}{\partial t} + \frac{\partial}{\partial x_j}\left(Du_j\right) = 0, \tag{1a}$$

$$\frac{\partial u_i}{\partial t} + u_j\frac{\partial u_i}{\partial x_j} = -g\frac{\partial z_s}{\partial x_i} - \frac{1}{\rho D}\frac{\partial}{\partial x_j}\left(S'_{ij} - S''_{ij}\right) - \frac{\tau_{bi}}{\rho D}, \tag{1b}$$

$$\frac{\partial E}{\partial t} + \frac{\partial}{\partial x_j}\left((u_j + c_{gj})E\right) + S'_{ij}\frac{\partial u_j}{\partial x_i} = -\mathcal{D}, \tag{1c}$$

$$\frac{\partial \Phi}{\partial t} + \varpi + u_j\frac{\partial \Phi}{\partial x_j} = 0, \tag{1d}$$

$$\frac{\partial z_b}{\partial t} + \frac{1}{1-p}\frac{\partial q_j}{\partial x_j} = 0, \tag{1e}$$

where $z_s(x_1, x_2, t)$ is the mean sea level, $z_b(x_1, x_2, t)$ is the mean bed level, $D(x_1, x_2, t)$ is the total mean depth ($D = z_s - z_b$), $\vec{u}(x_1, x_2, t)$ is depth averaged current ($\vec{u} = (u_1, u_2)$) and $E(x_1, x_2, t)$ is the wave energy density. Other quantities are described below.

2.2. Waves

[14] The wave phase $\Phi(x_1, x_2, t)$ is defined through the wavenumber vector $\vec{K} = (K_1, K_2)$, such that

$$\nabla\Phi = \vec{K} \qquad \Phi_t = -\omega,$$

where ω is the absolute frequency (i.e., that apparent to a stationary observer), and

$$\varpi = \sqrt{gK \tanh KD} \, ,$$

where ϖ is the intrinsic frequency (that apparent to an observer moving with the current). For brevity we denote $|\vec{K}|$ as K from now on, and the corresponding magnitude of the group velocity vector as c_g, where $c_g = (c/2)(1 + 2KD/\sinh(2KD))$ and $c_{gi} = (K_i/K) c_g$. Similarly, the phase velocity c is given by linear theory [see, e.g., *Mei*, 1989].

[15] The wave energy dissipation model is that of *Thornton and Guza* [1983] and takes the form

$$\mathcal{D} = \frac{3\sqrt{\pi}}{16} B^3 f_p \rho g \frac{H_{\mathrm{rms}}^5}{\gamma_b^2 D^3} \left(1 - \frac{1}{\left(1 + (H_{rms}/\gamma_b D)^2 \right)^{5/2}} \right) ,$$

where $f_p \, (= \varpi/2\pi)$ is the intrinsic peak frequency of the wave field [see *Yu and Slinn*, 2003], $B \,(= 1.0)$ is a breaking related coefficient, $\gamma_b \,(= 0.42)$ is the breaker index, H_{rms} ($E = \frac{1}{8} \rho g H_{\mathrm{rms}}^2$) is root mean square average of the wave height, and ρ is the water density and g represents gravity. The waves drive the circulation through the radiation stress terms S'_{ij}.

2.3. Currents

[16] The wave-driven flow caused by the radiation stresses (S'_{ij}) is effected through the linear expressions [*Longuet-Higgins and Stewart*, 1964]

$$S'_{ij} = E \left(\frac{c_g}{c} \frac{K_i K_j}{K^2} + \left(\frac{c_g}{c} - \frac{1}{2} \right) \delta_{ij} \right),$$

where δ_{ij} is the Kronecker delta symbol. The Reynolds stresses (S'') are parameterized using a horizontal viscosity coefficient [*Battjes*, 1975],

$$S''_{ij} = \rho \nu_t D \left(\frac{\partial u_i}{\partial x_j} + \frac{\partial u_j}{\partial x_i} \right),$$

where $\nu_t = M \, (\mathcal{D}/\rho)^{\frac{1}{3}} H_{\mathrm{rms}}$ ($M = 1$ [see *Battjes*, 1975]). The bed shear stress $\vec{\tau}_b$ is parameterized through a linear friction law,

$$\vec{\tau}_b = \rho \mu \vec{u} \, , \qquad \mu = \left(\frac{2}{\pi} \right) c_D u_{\mathrm{rms}},$$

where $c_D = \left(\frac{0.40}{\ln (D/z_0) - 1} \right)^2$, $z_0 (= 0.01$ m) is the roughness length and u_{rms}, the root-mean-square wave orbital velocity at the boundary layer edge z_0, is computed through linear wave theory, i.e.,

$$u_{\mathrm{rms}} = \frac{H_{\mathrm{rms}}}{2} \frac{gK}{\varpi} \frac{\cosh Kz_0}{\cosh KD} .$$

2.4. Bed Change

[17] The sediment flux $\vec{q}$ is defined here on the basis of the formula of Soulsby and Van Rijn given by *Soulsby* [1997],

$$\vec{q}_{svr} = \alpha \left(\vec{u} - \gamma u_{\mathrm{rms}} \vec{\nabla} h \right), \tag{2}$$

where the stirring function α reads

$$\alpha = A_s \left[\left(|\vec{u}|^2 + \frac{0.018}{c_D} u_{\mathrm{rms}}^2 \right)^{1/2} - u_{\mathrm{crit}} \right]^{2.4} ,$$
$$\text{if} \left(|\vec{u}|^2 + \frac{0.018}{c_D} u_{\mathrm{rms}}^2 \right)^{1/2} > u_{\mathrm{crit}} \tag{3}$$
$$\alpha = 0 \, , \qquad \text{otherwise.}$$

There are various parameters in this model. $A_s = A_{ss} + A_{sb}$ where A_{ss} represents the suspended load and A_{sb} the bedload; and u_{crit} the threshold flow intensity for sediment transport, which depends on sediment properties and depth. The full expressions for these quantities are given by *Soulsby* [1997] and we include them in the perturbation expansion. Finally, $p \,(= 0.4)$ is the seabed porosity and $\gamma \,(= 1.6)$ is a morphodynamical diffusion coefficient. The original equation from *Soulsby* [1997] has been adapted for a two-dimensional flow and to model a gravitational downslope transport proportional to the bottom wave orbital velocity.

2.5. Basic State

[18] We assume that the basic state represents an equilibrium of our system, or at least is only developing over a significantly longer timescale than any emerging bed form, and so is time-invariant for the purposes of our study. The basic state is assumed to be an alongshore uniform beach profile, $z_b = -Z(x)$, with the accompanying flow and wave field, $\vec{u} = (0, V_0(x))$, $E = E_0(x)$ and $\Phi = \Phi_0(x, t)$. To calculate the basic state we solve numerically the time- and alongshore-independent equations (1a)−(1d) determining the wave-driven hydrodynamics corresponding to a fixed bottom profile.

[19] Consistent with this level of complexity we choose to analyze the analytically smooth beach profile that includes a shore-parallel bar of *Yu and Slinn* [2003], which is representative of some profiles found at existing natural coasts (Duck, North Carolina),

$$Z(x) = a_1 \left(1 - \frac{\beta_2}{\beta_1} \right) \tanh \left(\frac{\beta_1 x}{a_1} \right) + \beta_2 x$$
$$- A_b \exp \left[-W_b \left(\frac{x - X_b}{X_b} \right)^2 \right], \tag{4}$$

where X_b is the bar location, W_b its width and A_b its amplitude. Note that equation (4) possesses a shoreline slope β_1 and an offshore slope β_2.

[20] Hereinafter we examine three bathymetric configurations corresponding to the alongshore bar positioned at different distances from the shoreline, but keeping the overall slope of the beach the same in all cases. In Table 1 the parameters corresponding to these three profiles are given. The water depth on the crest, $h(x_b)$, increases for the bar location farther offshore, consistent with a bar migrating offshore under more severe conditions. Note that although the bars were originally located at distances of 50, 80 and 120 m from the still water shoreline ($x = 0$), there is inundation due to set-up and this effectively increases the bar crest to shoreline distance X_b, with the shoreline now at $x = x_0$, where $D_0 = D(x_0) \sim 10$ cm, which defines the onshore boundary of the basic state. At $x = 0$ the alongshore

Table 1. Characteristics of the Basic State Bed Profiles

Profile	β_1	β_2	a_1, m	X_b, m	A_b, m	W_b, m	$h(x_b)$, m	h_∞, m
1	0.075	0.0064	2.97	50.0	1.5	5.0	1.14	28.3
2	0.075	0.0064	2.97	80.0	1.5	5.0	1.63	28.3
3	0.075	0.0064	2.97	120.0	1.5	5.0	1.97	28.3

velocity is set to be zero. Since the governing equations (1a), (1c) and (1d) are first order, no more boundary conditions at $x = x_0$ are needed. Approximately 4000 m from the coast, where the depth is $\approx$28 m, the bottom profile is taken as constant, and hydrodynamic variables take offshore values. Figure 2 shows an example of a basic state for the beach profile 2 and moderate wave conditions incident at a small offshore angle.

2.6. Linear Stability Analysis

[21] The approach we take is standard for linear stability models: We linearize with respect to a basic state. The six dependent variables are therefore expressed as a basic state (equilibrium) quantity plus a perturbation about that equilibrium, $[\eta, h, u, v, e, \phi]^T$, such that

$$z_s = \eta_0(x) + \eta(x, y, t),$$

$$z_b = -Z(x) + h(x, y, t),$$

$$u_1 = u(x, y, t),$$

$$u_2 = V_0(x) + v(x, y, t),$$

$$E = E_0(x) + e(x, y, t),$$

$$\Phi = \Phi_0(x, t) + \phi(x, y, t),$$

and where

$$D = \eta_0(x) + Z(x) + (\eta(x, y, t) - h(x, y, t))$$
$$= D_0(x) + d(x, y, t).$$

[22] The perturbed quantities are assumed small with respect to those of the basic state, so that the resulting system of equations can be linearized with respect to this state (see *Dodd et al.* [2003] for an overview of this method in coastal morphodynamics). This linearization is straightforward but lengthy and the expressions of the full linearized model can be obtained upon request from the authors. Finally, we make use of the quasi-steady hypothesis, which implies that hydrodynamical instabilities are excluded by disregarding time derivatives of hydrodynamical quantities, so that the flow field responds (on the morphodynamical timescale) instantaneously to the bed evolution.

[23] Since the morphodynamic instability mechanism to be examined is confined close to the coast, suitable offshore boundary conditions are: $(u, v, \eta, h, e, \phi_x, \phi_y,) \rightarrow 0$, as $x \rightarrow \infty$. At the shoreline ($x = x_0$), considered fixed, a small finite depth is again allowed to avoid the singularity in $\nabla\phi$ for $D = 0$ and the complications of the swash zone. The latter are believed to be unimportant for the dynamics of the surf/shoaling zones, which is the aim of the model. Thus $(u, v, h) = 0$ is assumed at $x = x_0$. Since the governing equations for η, e and ϕ are first order, b.c.'s at $x =$

x_0 are not needed. Since the coefficients of the governing equations do not depend on y we can assume alongshore periodicity into our perturbations, so that

$$\Psi(x, y, t) = \psi(x)e^{\sigma t + iky}, \qquad (5)$$

where Ψ and ψ can represent any of our perturbation variables. Substituting (5) in (1a)–(1e) and imposing the boundary conditions results in a system of linear equations that defines an eigenvalue problem. It is solved numerically by a spectral method [see *Iranzo and Falqués*, 1992], which allows computational nodes to be distributed efficiently where variations are most rapid (typically near the shoreline). Experiments used 300 collocation points in the cross-shore direction, with half of the points located at the first 150 m, to achieve numerical convergence [*Iranzo and Falqués*, 1992; *Falqués et al.*, 1996]. The Fortran code to solve for the basic state and its linear stability is referred to as MORFO60.
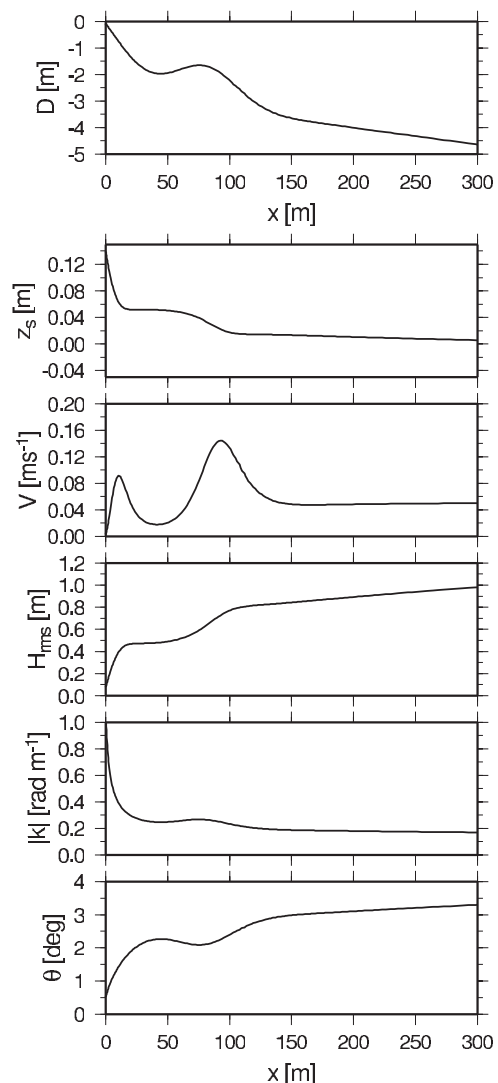

Figure 2. Variables of the basic state for the beach profile 2, $H_{rms\infty} = 1.5$ m, $T = 6$ s and $\theta_\infty = 5°$ as a function of the cross-shore coordinate x. From top to bottom: total depth, free surface elevation, alongshore velocity, root mean square wave height, wave number and angle of the wave fronts.
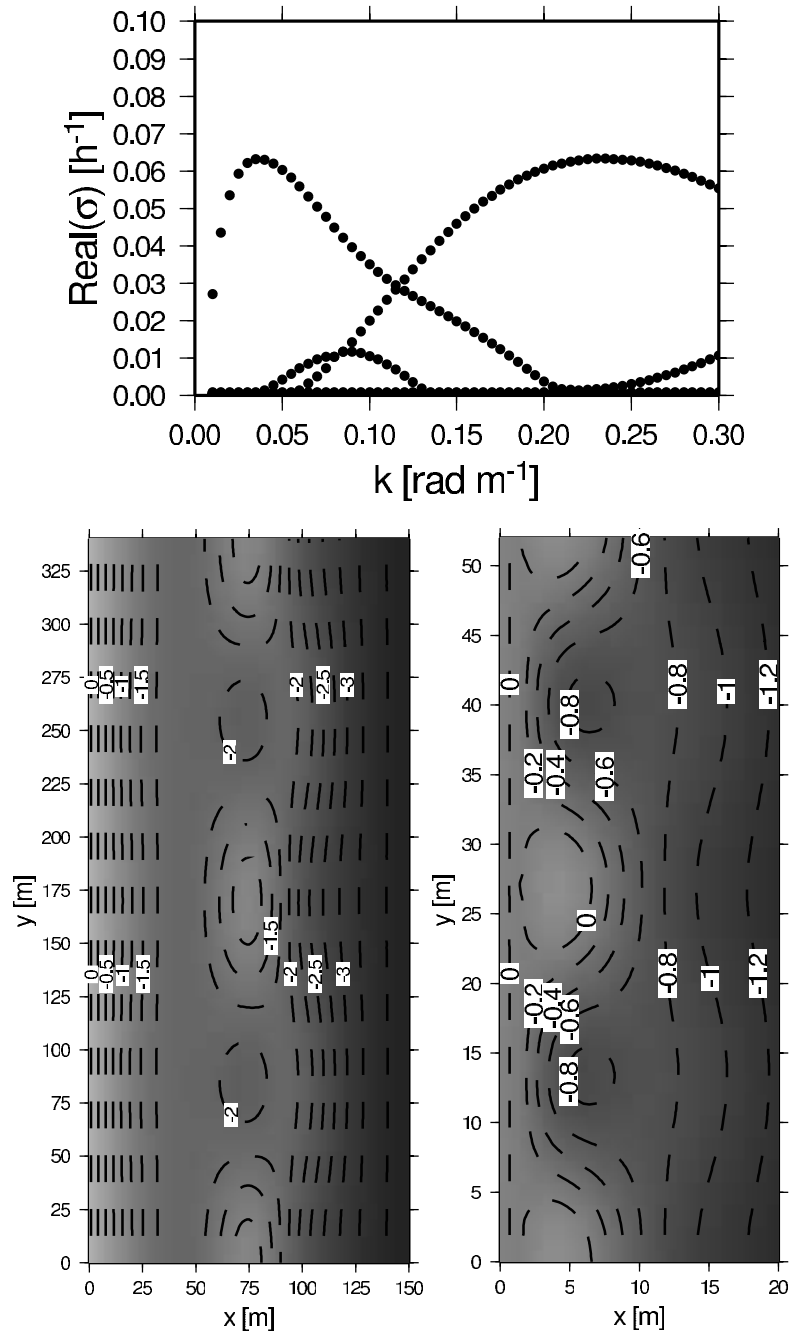
Figure 3. (top) Growth rate curve as a function of the wavenumber for beach profile 2, $H_{rms\infty}$ = 1.5 m, T = 6 s and θ_∞ = 0°. (bottom) Depth contours (light area are shoals) for the most unstable mode ((left) λ = 169 m, τ = 19 h and (right) λ = 27 m, τ = 16 h.

[24] For each alongshore wavenumber k as many eigenvalues σ and associated eigenfunctions $\psi(x)$ as degrees of freedom of the discretization are obtained. Many of them are purely numerical, i.e., not describing any solution of the continuous system of stability equations [*Iranzo and Falqués*, 1992; *Falqués et al.*, 1996]. Those which are physical and have Re(σ) > 0 represent a possible instability mode associated to the spatial pattern defined by k and $\psi(x)$. For each mode, the e-folding time is $\tau = 1/$Re(σ) and gives an indication of the characteristic formation time in nature. The alongshore migration speed is computed as $V_{mi} = -$Im(σ)/k. The growth rate curves show Re(σ) as a function

of k and allow identification, for each mode, of the wavelength with the largest growth rate: the fastest growing mode (FGM) which is interpreted as the predominant alongshore lengthscale for that particular mode.

[25] We reiterate that the approach taken is to obtain an alongshore-uniform basic state from equations (1a)–(1d) by prescribing $z_b = -Z(x)$ from equation (4), and then to use the perturbation model, derived from equations (1a)–(1e), the examine its stability.

[26] Typical growth rate curves which are relevant for our surf zone morphodynamic instability analysis are shown in Figure 3 for profile 2 and normally incident waves. The

Table 2. Wave Characteristics for All Sets of Experiments

$H_{rms\infty}$, m	T, s
0.5	4.0, 6.0, 12
1.0	4.0, 6.0, 12, 18
1.5	6.0, 12, 18
2.0	6.0, 12, 18
2.5	6.0, 12, 18

peaks in the growth rates indicate the alongshore spacings of the FGMs. The local maximum at $k = 0.0370$ rad m^{-1} ($\lambda = 169$ m) corresponds to the initial development of a crescentic bar/rip channel system of the alongshore bar (see Figure 3, bottom left) and has an e-folding time $\tau = 19$ h; the maximum at $k = 0.2350$ rad m^{-1} ($\lambda = 27$ m) corresponds to a transverse bar system at the shore (Figure 3, bottom
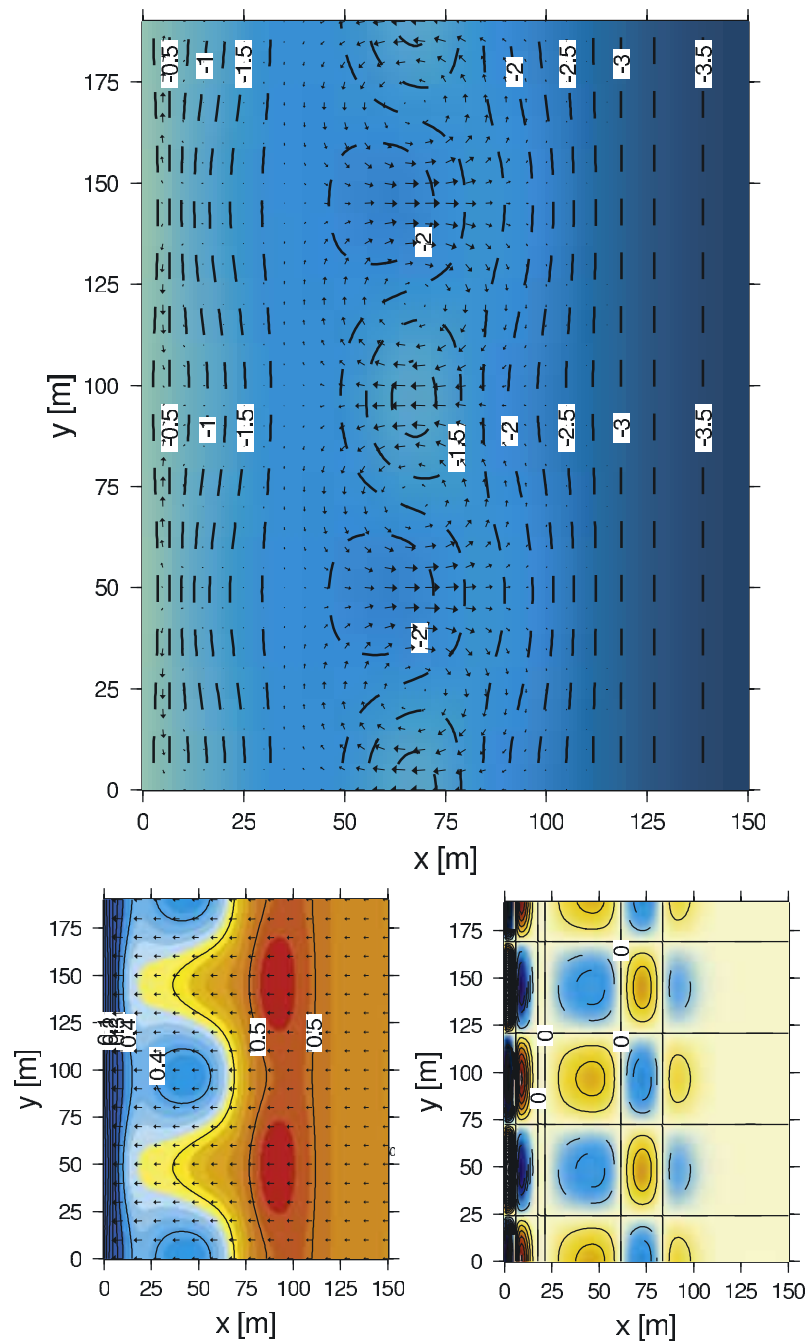
Figure 4. (top) Depth contours (light (dark) areas are shoals (pools)) and current vector, (bottom left) root mean square wave height (red (blue) areas imply higher (lower) wave height) and wavenumber vector, and (bottom right) free surface elevation perturbation (red (blue) areas are elevations (depressions)), for the fastest growing mode (FGM) ($\lambda = 97$ m, $\tau = 92$ h) for $\theta_\infty = 0°$, $H_{rms\infty} = 0.5$ m, $T = 6.0$ s and for profile 2.
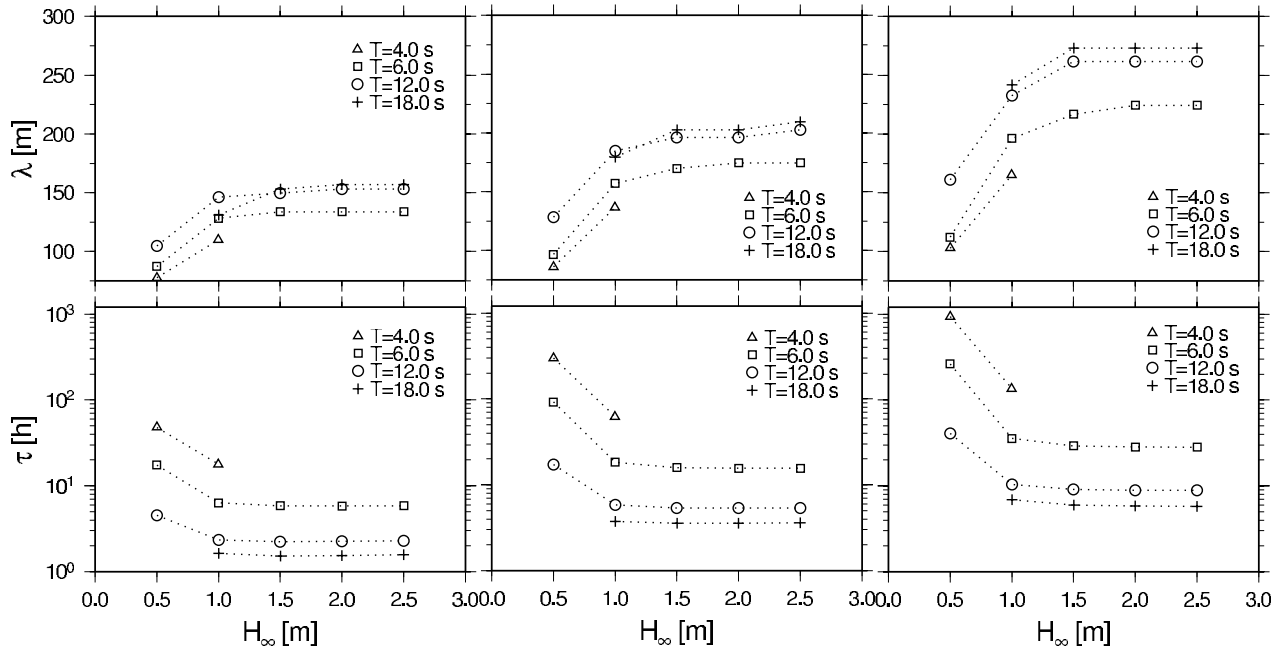
Figure 5. (top) Alongshore spacing and (bottom) *e*-folding time of the FGM for $\theta_\infty = 0°$ and $d_{50} = 2.0 \times 10^{-4}$ m. Profiles 1, 2 and 3 on left, middle and right, respectively.

right) with $\tau = 16$ h. Accordingly, we may expect these patterns to more than double in size in these time-frames. The main interest here is the evolving rip channel systems, so unless otherwise stated we focus our attention on these features. For visualization purposes variables are plotted with a bottom perturbation amplitude of 0.5 m.

3. Crescentic Bar/Rip Channel Development

[27] It is important to realize that our study gives qualitative insight along with some quantitative predictions but is limited by the assumptions underpinning linear stability analysis: only the initial development is examined. In order to obtain a reasonably representative set of experiments to investigate the growth of rip channel systems we vary wave height and period, the sediment size, and the offshore angle of incidence for each of the three profiles. We vary the offshore wave height ($H_{\mathrm{rms}\infty}$) between 0.5 and 2.5 m to examine a range of conditions from low energy through to heavier seas. Similarly, we examine a realistic range of wind through swell seas varying the period (T) from 4 s to 18 s. In Table 2 the combinations of wave heights and periods used are shown. Also of interest is the sensitivity of results to changes in the grain size and in the threshold velocity of sediment movement. In order to check the effects of wave refraction, we examine experiments excluding the perturbations in the wave phase from the governing equations. We also investigate the effect of slightly off-normal incidence (5°). The reference grain size is $d_{50} = 2.0 \times 10^{-4}$ m (medium sand [*Soulsby*, 1997]). Other model parameters (breaking coefficient B, breaker index γ_b or the roughness length z_0) have not been varied. The values used here are standard in the literature and small changes within acceptable limits lead to similarly small quantitative changes. In the explo-

rations in the alongshore wavenumber the increment in k is 0.001 rad m^{-1}.

3.1. Experiments at Normal Wave Incidence

[28] For each of the bed profiles of Table 1 and wave conditions of Table 2 with $\theta_\infty = 0°$ we find the basic state and then solve the stability problem. As can be seen in Figure 4, the eigensolutions represent a growing crescentic bar/rip channel system. The offshore flow in the channel can be clearly seen, as well as the region of deposition a little farther offshore, as the flow decelerates. The onshore flow over the shoals is just as concentrated as that offshore, a consequence of the linearity of the model. These rip cells are a robust feature of the experiments, and occur for all bar locations. The waves penetrate into the channels, whereas the presence of the shoal dissipates most of the wave energy.

[29] Note also in Figure 4 the presence of small circulation cells close to the shore with opposite rotation to the rip cells. These shoreline circulation cells tend to be accompanied by bed forms in the inner surf zone. These inner shoals and channels are in phase with the rip channels and shoals at the bar. The inner bed forms are prominent under lower energy wave conditions and disappear for medium and high energy conditions. The presence of counter-rip-rotating cells is associated with low and medium energy conditions. For high energy conditions a single circulation cell (the rip cell) is present, and for the largest energy conditions the cell extends up to the shoreline.

[30] Figure 5 summarizes the alongshore spacings and *e*-folding times of the FGM for all the experiments. In general, as the bar position moves offshore (and the depth of water on the bar increases) the spacings and the *e*-folding times increase (so the bed forms grow more slowly) for the same wave conditions. For the same profile the
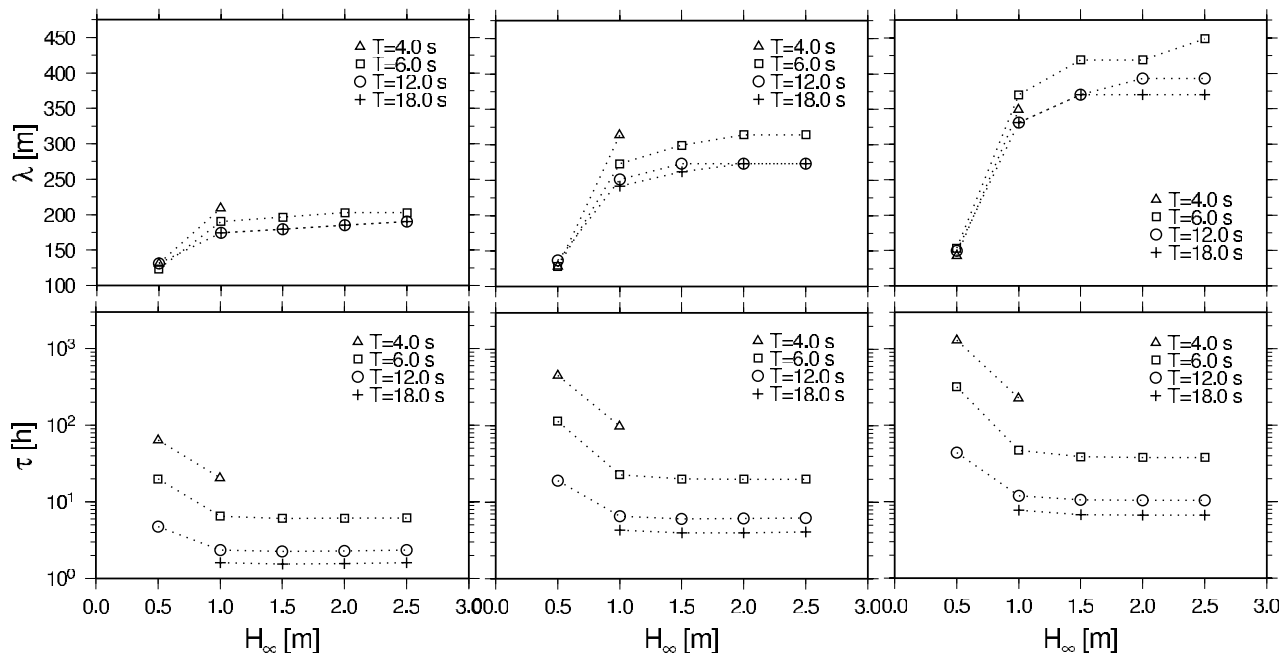
Figure 6. (top) Alongshore spacing and (bottom) *e*-folding time of the fastest growing mode for $\theta_\infty = 5°$ and $d_{50} = 2.0 \times 10^{-4}$ m. Profiles 1, 2 and 3 on left, middle and right, respectively.

spacings increase with increasing offshore wave height and period, whereas *e*-folding times decrease. A more detailed discussion is presented in the next section.

3.2. Experiments at Oblique Wave Incidence

[31] Since waves are rarely exactly normally incident, we now examine the effect of slightly off-normal wave incidence on the rip channel formation. Here, therefore, we perform experiments for the same cases as normal incidence but for $\theta_\infty = 5°$: see Figure 6, and compare with Figure 5, altered, particularly for the 4 s and 6 s wave. In fact, the alongshore spacings increase typically by 20 and 60% when compared with the equivalent normal cases, with the larger wave heights and smaller period and the most offshore bar showing the largest change. The result is that largest spacings now develop for the shorter wave periods and not the longer periods (as for normal incidence), although the longer period features still grow faster (see section 4.1). Note also that at 5° incidence, for longer period waves spacings appear to reach a limiting value. The move to off-normal incidence reveals a small amount of obliquity in the cells (see Figure 7), and, additionally, a small longshore current in the basic state. For example, the longshore current at the bar position for profile 2 and $H_{\mathrm{rms}\infty} = 2.5$ m is $V_b = 0.108$ m s^{-1}, $V_b = 0.090$ m s^{-1} and $V_b = 0.090$ m s^{-1}, for, respectively, $T = 6.0$ s $T = 12.0$ s and $T = 18.0$ s. Owing to the longshore current these patterns have an alongshore migration rate (V_m) that ranges from a few centimeters per hour to a maximum of 5 m h^{-1} for larger wave energies; see also Figure 15 in section 4.

3.3. Experiments Varying Sediment Properties

[32] Results of experiments with a smaller ($d_{50} = 1.0 \times 10^{-4}$ m) and larger ($d_{50} = 5.0 \times 10^{-4}$ m) grain sizes, and no critical bed shear stress threshold ($u_{\mathrm{crit}} = 0$ in equation (2)

are presented in Figure 8. Figure 8 only shows results for profile 2 as these are representative of those for the other two profiles. Smaller grain sizes yield a more mobile bed and therefore smaller *e*-folding times (uniformly reduced by a factor 0.6), while larger grain size experiments lead to a less erodible bed and larger values for τ (increase by a factor 1.2). The calculations presented in Figure 5 (and Figure 6) impose a critical bed shear stress threshold on sediment movement through (2). The effect is to make the sediment less mobile. Removal of this threshold yields a reduction in τ by about a factor 0.5. The alongshore spacing of the FGMs remains almost unchanged.

3.4. Experiments Without Phase Perturbations

[33] A final set of experiments with a modified version of the model that excludes phase perturbations (and therefore refraction on emerging bed forms) are presented. We use the same cases and parameters as section 3.1. Figure 9 summarizes results for profile 2. Both alongshore spacings and *e*-folding times are similar, although smaller by a factor up to 0.7 to those obtained including phase perturbations (see Figure 5 (middle) in section 3.1). The overall shape of the patterns (see Figure 10 (top)), is also similar to those obtained with the complete model: the rip channel/crescentic bar system. There are several differences, however: The bed perturbation extends farther offshore as a kind of transverse bar (compare (see Figure 10 (top)) with Figure 4), and it is accompanied by more energetic currents. The shoreline associated bed perturbations are also less prominent and rarer, and, in the cases where they appeared before, the double circulation cells are now much weaker. The alongshore variations of the wave energy are weaker as well.

[34] Lastly, we present in Figure 10 (bottom) a hydrodynamic (current and waves) computation using the full
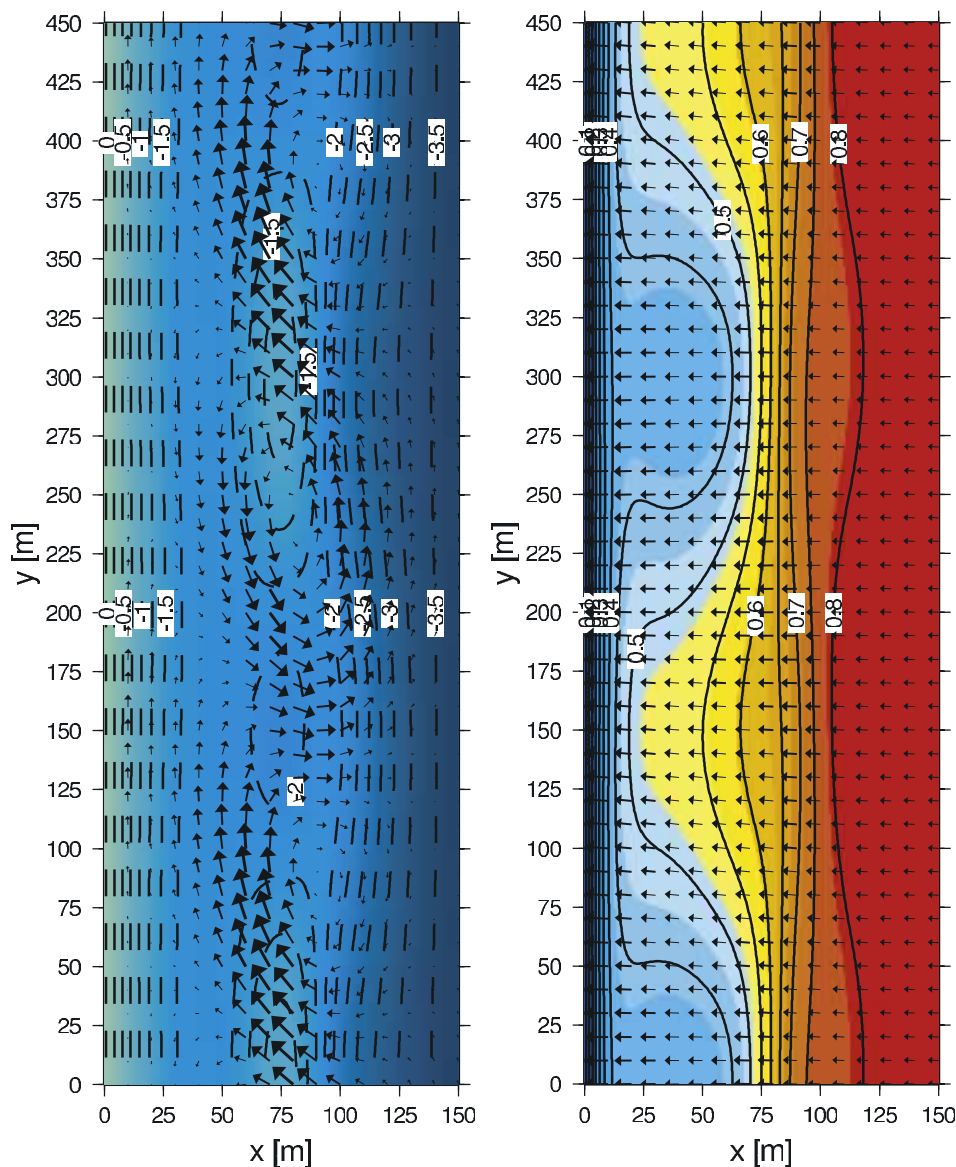
Figure 7. (left) Depth contours and current vector and (right) root mean square wave height and wavenumber vector, for the most unstable mode ($\lambda = 300$ m, $\tau = 20$ h, $V_m = 1.5$ m h^{-1}) of $\theta_\infty = 5°$, $H_{rms\infty} = 1.5$ m, $T = 6.0$ s and for profile 2.

model, for the most unstable bed perturbation obtained using the model without phase perturbations. Note that the conceptual difference between the top and bottom plots of Figure 10 is that the top one corresponds to a coupled bottom and hydrodynamics (excluding refraction) and leads to an FGM and therefore an evolving bed; the lower one is the resulting hydrodynamics (including refraction) for a fixed topography (with the aforementioned 0.5 m amplitude perturbation), and so does not produce the sediment transport that leads to the FGM. If we were to run the model without refraction on the same fixed bathymetry we would recover the circulation pattern shown in Figure 10 (top). Looking at the lower figure, however, we can see noticeable differences, most particularly in the shoreline circulation cells (now much enhanced) and the "transverse bar" circulation farther offshore (now diminished with respect to the other patterns). Note also the apparently greater

focusing of the waves in the rip channels. We shall return to this computation in the next section.

4. Discussion

4.1. Growth of Crescentic Bars

[35] Figure 11 shows the wave breaking dissipation patterns corresponding to some of the model results. The plots are reminiscent of the Argus video images of crescentic bars indicating a good qualitative agreement with observations. The bottom contour lines are also shown in these plots and a good correlation can be seen between the dissipation patterns and the topography at the outer breaking zone over the bar, in particular more intense breaking on the bar for larger H_{rms}.

[36] As can be seen by comparing Figures 2 and 12 the maximum in potential stirring is seaward of the bar.
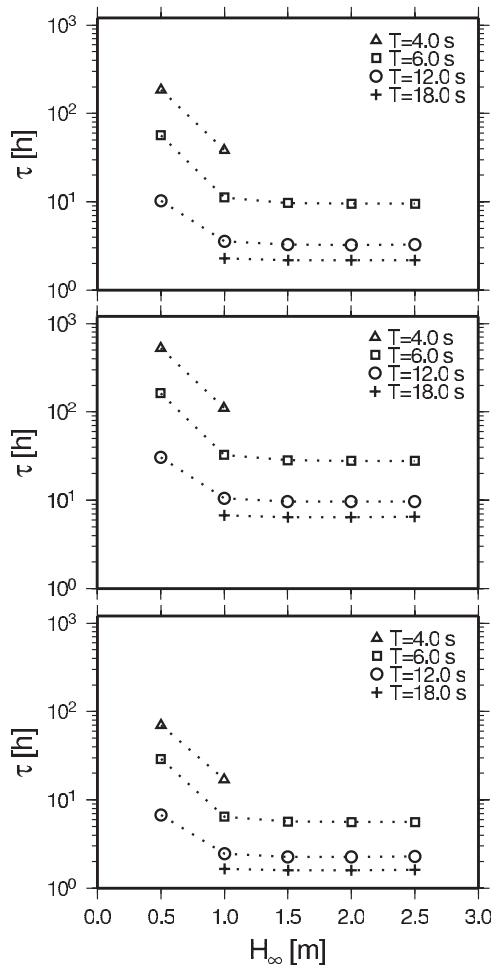
tions of λ/X_b are within the range of values given by all the models in the case of normal incidence, i.e., from 1 to 4, regardless of whether they are based on linear stability analysis or nonlinear studies [*Deigaard et al.*, 1999; *Damgaard et al.*, 2002; *Coco et al.*, 2003; *Reniers et al.*, 2004; *Castelle*, 2004]. The spacings are larger for oblique incidence than for normal incidence by a factor ranging from 1.2 to 2 when jumping from $\theta = 0$ to $\theta = 5°$. Significantly larger spacings up to $\lambda/X_b \sim 10$ are found for $\theta \sim 25–30°$. This is consistent with *Deigaard et al.* [1999]. However, their results showing a very strong increase in λ from $\theta = 0$ to $\theta = 10°$ and suggesting that the exact normal incidence was some sort of singularity have not been obtained. Instead, a gradual and almost linear increase in spacing is found from $\theta = 0$ to $\theta \sim 30°$; see Figure 15.

4.1.2. Wave Period

[38] The influence of wave period on the spacing depends on the angle of incidence (normal or slightly off-normal). For normal incidence spacings increase for increasing period, whereas the spacings decrease with period for small oblique incidence. The effects of wave period can be understood from shoaling processes which lead to different energy distribution for different wave periods. This affects in turn the stirring function (α/D), as can be seen in Figure 12. For the same offshore wave energy, large periods produce larger sediment transport and larger gradients in the potential stirring function, because of their longer wavelength and therefore greater potential to move sediment. The trend for oblique incidence may be explained by the larger refraction that longer period waves will undergo for equivalent beach conditions. The 6 s wave will break when the waves are at a larger angle to the shore than will either the 12 s or 18 s waves. This results in a larger longshore current
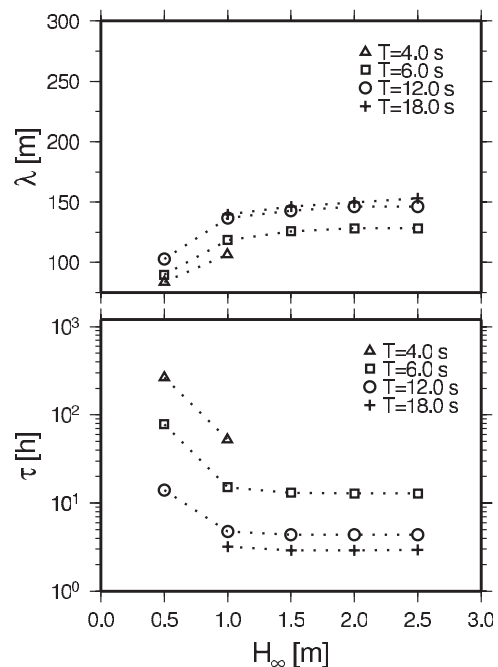
Figure 8. The *e*-folding time of the fastest growing mode for $\theta_\infty = 0°$ and profile 2 for (top) $d_{50} = 1.0 \times 10^{-4}$ m, (middle) $d_{50} = 5.0 \times 10^{-4}$ m and (bottom) $u_{crit} = 0$ (with $d_{50} = 2.0 \times 10^{-4}$ m).

According to *Falqués et al.* [2000] (see section 1), this is the situation in which an offshore (onshore) flowing current produces erosion (accretion) so that a positive feedback between crescentic bar morphology and the rip current cells occurs. Thus the present results with a more sophisticated model corroborate the earlier findings concerning the bed-surf coupling as the origin of crescentic bars with the associated circulation [see *Deigaard et al.*, 1999; *Falqués et al.*, 2000].

4.1.1. Spacings

[37] As can be seen in Figure 13, and consistent with previous work [see, e.g., *Deigaard*, 1990; *Damgaard et al.*, 2002; *Calvete et al.*, 2003], we find a roughly linear increase in spacing, λ, with X_b. For fixed X_b, the spacing increases with increasing wave height, H_{rms}, but saturates for large waves (see Figures 5 and 6). This can be understood from Figure 14, where H_{rms} at the bar crest for the basic state is plotted for different offshore wave heights. It is seen that H_{rms} at the bar increases with offshore wave height until a saturation is reached when wave energy is primarily dissipated offshore of the bar. The spacings for normal incidence are about $1.5–2\ X_b$ for low energy conditions and about $2–4\ X_b$ for higher energy conditions. These predic-

Figure 9. (top) Alongshore spacing and (bottom) *e*-folding time of the fastest growing mode for $\theta_\infty = 0°$, $d_{50} = 2.0 \times 10^{-4}$ m and profile 2 of the model that excludes phase perturbations.
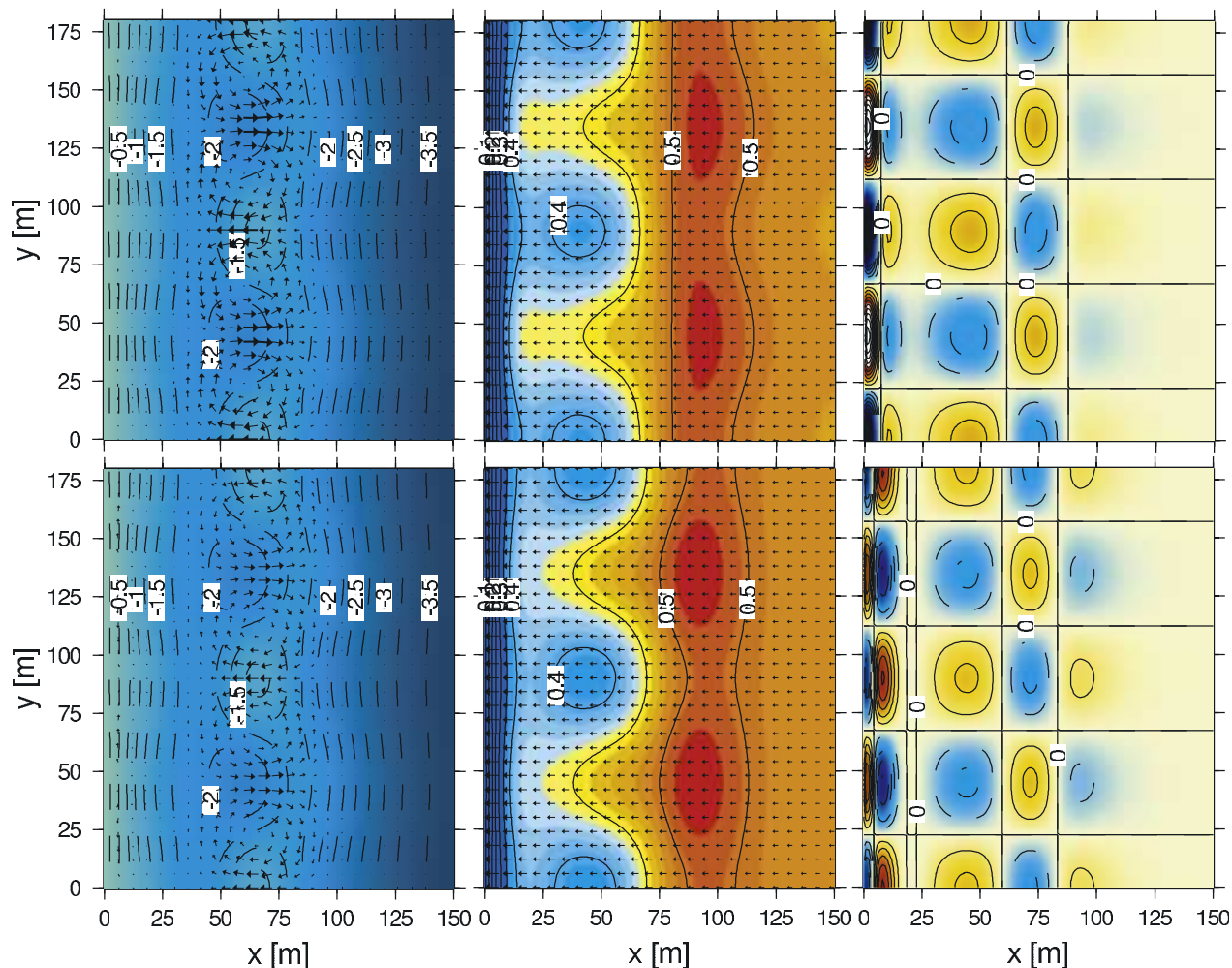
Figure 10. (left) Depth contours and current vector, (middle) root mean square wave height and wavenumber vector, and (right) free surface perturbation (red (blue) areas are elevations (depressions)). (top) The most unstable mode ($\lambda = 90$ m, $\tau = 78$ h) of $\theta_\infty = 0°$, $H_{rms\infty} = 0.5$ m, $T = 6.0$ s and for profile 2 of the model that excludes phase perturbations. (bottom) Perturbations computed with the model with phase perturbations but with the bathymetry above imposed and fixed (so the calculation is that of a flow responding to a non-evolving bed).

which in turn may be responsible for the larger spacings, see Figure 15. The larger spacings for long period waves for normal incidence may be linked to the breakpoint moving slightly farther offshore, and therefore increasing the effective X_b (note that increased spacing, though significant, is smaller than the increase between the different profiles).

4.1.3. Growth Times

[39] The e-folding times in the present model are generally similar to the characteristic times of *Reniers et al.* [2004] (~3 days) and also similar or somewhat larger than those obtained by *Deigaard et al.* [1999] (8–12 hours). All these are, however, significantly smaller than those obtained by *Klein et al.* [2003] (~30 days), *Castelle* [2004] and *Damgaard et al.* [2002] (~15 days). In the latter study this could be due to the fact that their growth rates were strongly influenced by the large (constant) eddy viscosity needed for the nonlinear model experiments. More significant is that the trend obtained here, increase in e-folding time with increasing X_b, is opposite to that obtained by *Damgaard et*

al. [2002]. This may possibly be explained by the simpler stability model used in that study, but more likely it is due to the three beach profiles they examined, which possess progressively steeper local offshore bar slopes for larger X_b (to preserve $h(x_b)$). This acts to concentrate breaking more and can be seen in the plots of their stirring function.

[40] By increasing the incidence angle, e-folding times increase and for some cases (e.g., $T = 4$ or 6 s and $H_{rms} = 1.5$ m on profile 2) instability may totally disappear (negative growth rates). This is qualitatively consistent with *Deigaard et al.* [1999] who found increasing growing times for increasing obliquity. Also, results of *Castelle* [2004] with a nonlinear morphodynamic model suggested that significantly oblique incidence is less conducive to crescentic bars.

[41] Variations in the grain size and critical threshold of movement do not affect results significantly and they are as expected: smaller (larger) grain sizes lead to a more (less) erodible bed and therefore smaller (larger) e-folding times.
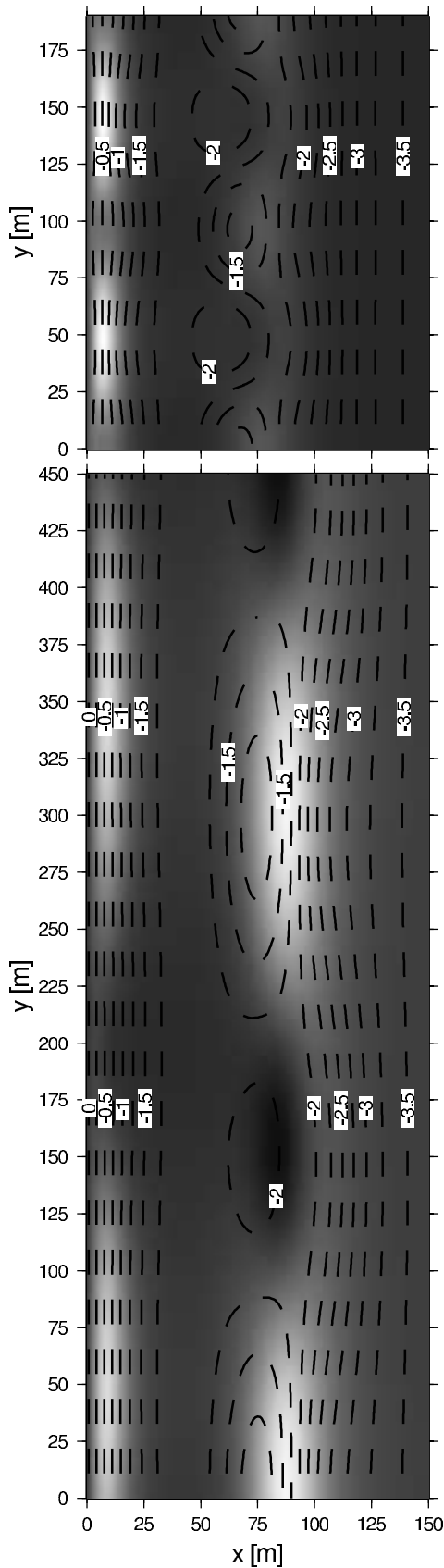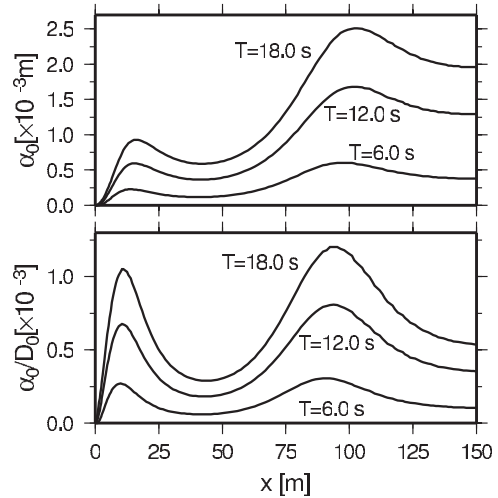
Figure 12. (top) Stirring function and (bottom) potential stirring of the basic state for the beach profile 2, $H_{\mathrm{rms}\infty} = 1.5$ m and $\theta_\infty = 0°$ for the different wave periods.

Similarly, no threshold of movement ($u_{\mathrm{rms}} = 0$) leads to a more erodible bed. Alongshore spacings remain almost unchanged.

4.2. Comparison With Observations

[42] Comparison of model results with observations of spacing is quite difficult. First, most observations of crescentic bars in the field are reported without information on the associated waves and currents. Recent exceptions to this are the work of *van Enckevort et al.* [2004] and *Castelle* [2004]. However, even in these cases the data sets are not complete, for example, the wave angle sometimes being unavailable. In addition, crescentic bars are detected by Argus video images when they already have a significant topographic signal.

[43] Whether or not linear stability analysis is adequate to describe them at this stage is unclear. As discussed by *van Enckevort et al.* [2004], the actual observed spacing is the result of complex self-organized processes that are induced by the changing wave conditions and which include merging and splitting of individual crescents. It is therefore
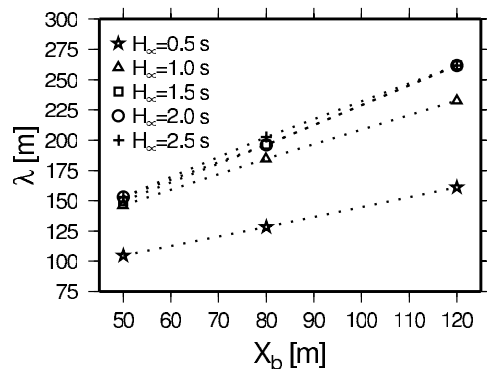

Figure 13. Alongshore spacing of the FGM as a function of the bar position for $T = 12.0$ s, $\theta_\infty = 0°$ and $d_{50} = 2.0 \times 10^{-4}$ m.

Figure 11. Dissipation patterns (light areas corresponds to larger dissipation) for the most unstable mode: (top) $\theta_\infty = 0°$, $H_{\mathrm{rms}\infty} = 0.5$ m, $T = 6.0$ s and for profile 2, and (bottom) $\theta_\infty = 5°$, $H_{\mathrm{rms}\infty} = 1.5$ m, $T = 6.0$ s and for profile 2.
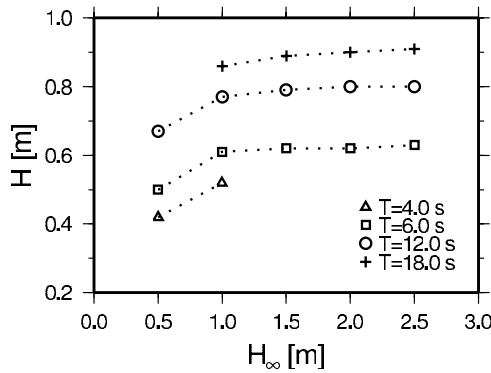
Figure 14. H_{rms} at the bar position of the basic state for beach profile 2 and $\theta_\infty = 0°$ as a function $H_{rms\infty}$.

argued that a nonlinear model is better suited for comparison against field observations than a linear stability model.

4.2.1. Linear Stability Analysis

[44] A linear stability model allows for a systematic study of parametric trends via a large number of runs which would be prohibitive for a nonlinear model. The basic point is that the system tries to adapt itself to its optimum spacing under the given wave conditions. How this adaptation takes place (including merging and splitting) depends on initial conditions and on the temporal behavior of the forcing and needs a nonlinear model for a description, but the basic physics and trends can be understood and predicted by the linear stability analysis. In the limit of very small amplitude, the optimum spacing is λ_{FGM}, the wavelength of the FGM. According to a nonlinear stability analysis [see, e.g., *Calvete and de Swart*, 2003] the optimum spacing might shift from λ_{FGM} to a subharmonic if the amplitude is large enough. Nevertheless, this optimum spacing is proportional to λ_{FGM}. The fact that after the peak of a storm λ is much larger than a few days later is a consequence of the fact that λ_{FGM} is larger for larger X_b and larger H_{rms}. The subsequent splitting for decaying wave energy occurs because the system tries to adapt to a new optimum spacing which is smaller because H_{rms} and X_b have decreased too as the bar has migrated onshore. A moderate increase of wave energy may turn around the process and merging of crescentic bars may occur.

4.2.2. Field Observations

[45] In addition to the basic physics, the linear stability analysis gives quantitative predictions of λ_{FGM} which can be compared to observations. In general, the range of observed spacings in the literature is so wide, $\lambda/X_b \sim 1-10$, that the predictions of all instability models fall within it. More detailed observations are needed in order to check the applicability of each model. Interestingly, *van Enckevort et al.* [2004] have measured the initial formation of crescentic bars at various beaches and hence provide an ideal data set to check the models. The observed λ/X_b ratios for the incipient crescentic bars were about 7–10, i.e., significantly larger than predictions by models for normal incidence (1–4). These large spacings are found only for oblique incidence in the present model and by *Deigaard et al.* [1999]. This is somewhat surprising since it would suggest that the observed formation of crescentic bars at

Duck, Miyazaki and Gold Coast occurs always for oblique wave incidence. Unfortunately, wave angle information is not always available. It is, however, reasonable to suppose that the probability of exact normal incidence (in deep water) is extremely low and that 'normal' incidence at breaking might usually correspond to a small obliquity in deep water. In contrast, observations from the Aquitaine coast described in *Castelle* [2004] show $\lambda/X_b \sim 1-4$, even for clear oblique incidence. This is, however, the mature spacing, probably long after the initial formation, and is consistent with the range $2-6$ observed by *van Enckevort et al.* [2004].

[46] The e-folding time (τ) increases for increasing X_b and wave angle, and for decreasing wave energy. For high energy conditions τ ranges from about 4 hours up to $2-3$ days. This is consistent with *van Enckevort et al.* [2004], who observed a period of $1-3$ days between the peak of the storm and the detection of crescentic shapes from Argus images. The
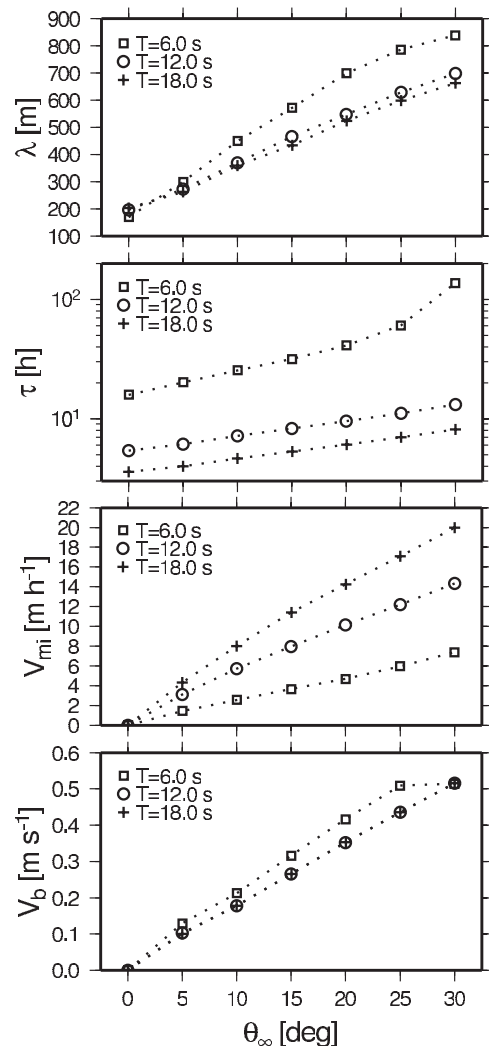

Figure 15. (top to bottom) Alongshore spacing, e-folding time and migration speed of the fastest growing mode, and longshore current of the basic state at the bar position as a function of θ_∞, for $H_{rms\infty} = 1.5$ m, $d_{50} = 2.0 \times 10^{-4}$ m and profiles 2.

e-folding time is, however, of several days for low energy. The latter implies that the formation of the crescentic bars/rip channel system will occur after a persistent long period of low/mild energy conditions. For very low energy and short periods, however, τ values are so large (several weeks) that there is probably no effective instability.

4.3. Circulation Cells, Megacusps, and Refraction

[47] As mentioned earlier, a feature of many of our numerical experiments is the double circulation pattern. As can be seen in Figure 4, this consists of the rip cells themselves and a counter-rotating system located near the shoreline. As wave heights increase this pattern persists but noticeably weakens, until it is no longer discernible for moderate wave conditions. It is important to remark that with the simplified stability model, in which the feedback onto the wave phase (and therefore onto wave refraction and shoaling) has been excluded, this secondary circulation weakens considerably. The secondary circulation has also been observed in the laboratory experiments by *Haller et al.* [2002] and in the numerical simulations by *Yu and Slinn* [2003] on topographically generated rip currents.

[48] The physical mechanism driving these shoreline circulation cells can be understood by looking at the wave set-up gradients. The set-up associated with rip cells and shoreline cells is shown in Figure 4. The stronger wave dissipation on the shoals on the bar creates a higher setup behind the shoals than at the channels. Therefore waves propagating through the channels are higher than those shoreward of the shoals. Thus wave breaking at the shore is more intense in front of the channels than in front of the shoals causing a higher set-up at the portion of the shoreline in front of the rip channels [*Wright and Short*, 1984; *Haller et al.*, 2002]. This double row of alternating maxima and minima in set-up is the pattern that would be in balance with the cross-shore gradients in S_{xx}. However, as is easily seen, the alongshore gradients in S_{yy} cannot balance the pressure gradients (because of the factor 3 due to the anisotropy originated by wave propagation) and alongshore currents flowing from the maxima in set-up to the minima are thus generated. This diminishes the water level at the maxima and increases it at the minima with the result that the cross-shore momentum balance is broken and cross-shore flows appear, from the minima in set-up to the maxima. Why the secondary cell weakens and eventually disappears for high energy conditions is still unclear.

[49] The shoreline circulation cells are usually accompanied by bed forms in the inner surf zone which are in phase with the crescentic bar, i.e., the shoals (troughs) being in front of the shoals (rip channels) on the bar (see Figure 4). These bed forms are more prominent under low wave energy conditions. *Calvete et al.* [2003] have demonstrated that these bars are forced by the hydrodynamics and are not part of the bed-surf morphodynamic coupling. Indeed, if sediment transport is switched off in the inner surf zone [see *Calvete et al.*, 2003] the circulation cells are still present while the bed forms are absent. At the cross-shore location of the bed forms, the gradient in potential stirring is onshore directed (Figure 12). In this situation, an offshore (onshore) current will produce accretion (erosion) [*Falqués et al.*, 2000]. Consistently, the shoals occur at the areas of offshore flow and the troughs at the areas of onshore flow.

[50] These features could be related to megacusps observed on natural beaches [*Wright and Short*, 1984]. If the shoreline was allowed to move in the model, the higher set-up in front of the rip channels would cause megacusp embayments. Furthermore, the topographic depression there, which is associated with the bed forms, would lead to erosion at the shore, i.e., reinforcement of the embayment at the shoreline. Similarly, the regions of lower set-up and shoals in the inner surf zone would correspond to megacusp horns. Since for low energy conditions shore-parallel bars move from a crescentic bar state to a transverse bar and rip state, we wonder if the megacusps obtained in the model could be the seed for the latter state in a nonlinear regime.

[51] Experiments without perturbations in the wave phase (i.e., no refraction on bed forms) reproduce the general trend and quantitative results as for the complete model; see Figure 10, top panel. However, the nearshore circulation cell and the corresponding morphological pattern is absent. This could be linked to the smaller alongshore gradients in wave energy (Figure 10, top panel) due to no focusing. Instead, an artificial bed perturbation appears in the offshore part of the bar, linked to an offshore flow. Subsequent inclusion of refraction on the immobile bathymetry (Figure 10, bottom panel) then suppresses this circulation, consistent with the (nonlinear) results obtained by *Yu and Slinn* [2003].

4.4. Transverse Bars

[52] In addition to the crescentic pattern on the bar, other instability modes emerge from the study. Formation of a transverse bar system at the shoreline is a robust feature of our results. As can be seen in Figure 3 the alongshore spacings are in the order of a few tens of meters. The offshore span of the bars is rather small, being about 10 m, so they are confined to the very inner surf zone where the gradient in potential stirring is offshore-directed. Similar to the rip channel system *e*-folding times decease for increasing wave energy conditions and for decreasing sediment size.

[53] This instability mode is also present when perturbations in the phase are excluded. This is in contrast with *Niederoda and Tanner* [1970] who suggested that the refraction of the waves by the transverse bars could be the main generating mechanism of such bars. Furthermore, *Caballeria et al.* [2002] have since confirmed this hypothesis with a nonlinear morphodynamic model, where the transverse bars grow as a positive feedback between flow and morphology with refraction being essential. The explanation for this disagreement could be that both the bars in that paper and here extend from the shoreline up to the first maximum in potential stirring, in a region where its gradient is offshore-directed. However, this maximum is located much farther offshore in the work of *Caballeria et al.* [2002] (it is imposed rather than being a result of the parameterization), so the bars in the present model have a much shorter length than those of *Caballeria et al.* [2002], which extend up to the breaking line. As was shown there, the importance of wave refraction on the bar dynamics depends on the cross-shore extent of the bed forms. For example, while little influence was found on the crescentic patterns which have a small extent at both sides of the breaking line, refraction was essential for the formation of

the long transverse bars that run from the shoreline up to the breaker line. The present results are, significantly, obtained on a barred beach profile, so our first maximum in potential stirring occurs close to the shore, thus limiting the length of the transverse bars, and reducing the importance of refraction. The nonlinear simulations of *Caballeria et al.* [2002] showed a complex dynamics with features sometimes developing close to the shoreline that might correspond to the linear instability mode found here. However, in the finite amplitude regime these features disappeared (or had relatively small amplitude) so that the final dominant patterns were always either the crescentic bars or the long transverse bars related to wave refraction. This could occur owing to a nonlinear interaction in which the offshore features would alter the inner surf zone hydrodynamics. This might also be the case in the work by *Reniers et al.* [2004] where those short transverse bars at the coastline do not form.

[54] For oblique incidence, the eigenvalues corresponding to transverse bars are not numerically convergent. Modifications in the discretization parameters are needed to describe properly the incipient oblique bar system at the shoreline. Accordingly, our conclusions only refer to the normally incident case.

4.5. Limitations

[55] The comparison with both observations and other models leads us to conclude that despite a number of simplifications the present model captures the main physics of crescentic bar formation on a barred beach. Some of these assumptions deserve some attention. Since the model disregards the cross-shore sediment transport directly associated with waves (undertow and wave asymmetry) the formation of the longshore bar itself or its cross-shore migration is not accounted for. Therefore the validity of the results are limited by the fact that during the rip channel formation the bar is assumed to keep its original position. Models where undertow was considered [*Reniers et al.*, 2004] do not give important differences regarding crescentic bar generation. Thus the authors suspect that the spacing of growing rip channel will only slowly adapt to the (unsteady) bar position.

[56] Another limitation of the model is that effects of diffraction and reflection are not taken into account either. Reflection could affect the formation of the shoreline bed forms, particularly for low energy conditions, when the shoreline features are more evident and when (short) wave reflection will be more prominent. It seems however unlikely that this process could impact on the bar region since dissipation is the main process there. Diffraction is not expected to be fundamental as the rip channel spacings are of the order of 100 m or more and the wavelength of the waves is of some tens of meters for the shorter period waves. Previous studies have shown that diffraction are typically small compared to shoaling and refraction processes [*O'Reilly and Guza*, 1993], albeit for random spectra. Perhaps some influence could be expected for the longer period waves where those length scales are closer each other. The directional spreading in the incident waves is not taken into account, and we expect a slightly increase in the alongshore lengthscale of the bed forms.

[57] Of more interest is the bar shape, especially in the light of comparisons with *Damgaard et al.* [2002]. The profile we use is, however, reasonably representative of real profiles at some locations, with a bar simply moved in the cross-shore direction. As a result we anticipate only quantitative changes with other profiles, but more fundamental differences cannot be ruled out, and studies on steeper/shallower beaches are likely to be useful.

5. Conclusions

[58] A linear stability model (MORFO60) based on depth-averaged shallow water equations of continuity, momentum, wave energy and phase transformation together with sediment conservation equation, has been set up. The model describes the dynamics of any small departure of the alongshore uniform equilibrium of a rectilinear coast either morphodynamic or purely hydrodynamic. It includes a comprehensive treatment of shoaling and surf zone hydrodynamics, including wave refraction on depth and currents and dissipation by breaking. The model has here mainly been applied to investigate the initial formation of rip currents and channels on a barred beach for normal or slightly off-normal wave incidence. The sediment transport has been modeled by using a total load formula with a depth dependent stirring function that includes threshold of motion and bedslope effects.

[59] Two instability modes have been examined in the present study, the first one describing the growth of rip channels and reshaping of the longshore bar to become crescentic, and the second one describing the growth of short transverse bars near the shoreline. The study focused on the first one but some attention has also been paid to the second.

[60] The results concerning the crescentic mode are generally consistent with previous studies by either linear or nonlinear stability analyses. This shows the robustness of the self-organized coupling between flow and morphology as the primary cause of crescentic bars. The present study, however, provides further insight in some aspects. First, a secondary circulation cell in counter-rotation to the rip circulation cell has been found close to the shoreline. This cell had been previously observed in laboratory experiments [*Haller et al.*, 2002] and in numerical simulations [*Yu and Slinn*, 2003]. This secondary circulation is more prominent for low energy conditions and it causes megacusp-like bed forms in phase with the crescentic bar morphology, horns in front of the shoals, embayments in front of the rip channels. These morphological features are not part of the morphodynamic feed-back leading to the crescentic bar but rather, they are forced by the circulation associated to the bar.

[61] A second aspect of the present investigation is a thorough parametric study of crescentic bar formation. It is found that the spacing between rip channels increases with increasing distance from bar crest to shoreline, X_b, and with increasing wave height. The latter trend saturates however for high energy conditions because the wave height at the bar saturates as a result of the increased dissipation offshore of the bar. At slightly off-normal wave incidence the spacings increase. Tests with quite oblique incidence reveal that, in contrast with previous suggestions that the exact normal incidence might be a singular limit, the spacing increases almost linearly with increasing incidence angle from 0 up to 30°. The spacings for normal incidence are

about 1.5–4 X_b whereas they can increase up to $\sim$10 X_b for quite oblique incidence, $\theta = 25{-}30°$. Though comparisons are not conclusive, model results show a good correspondence with observations. For instance, the spacing at the initial development stages described by *van Enckevort et al.* [2004] agrees with the model results for oblique incidence. Crescentic bars in other sites (probably mature bars) [*Castelle*, 2004] display shorter spacings, which are consistent with the model results for nearly normal incidence. The wave period also has an influence on the spacing, long periods causing longer spacings for normal incidence and shorter spacings for slightly off-normal incidence. It has been indicated how the tendency to merging/splitting of individual crescents according to the changing wave conditions, which is observed in the field, can be interpreted in terms of the present results for the crescentic mode.

[62] Typically, the *e*-folding times for the crescentic mode range from about 6 hours up to a few days which is consistent with the initial development of crescentic bars reported by *van Enckevort et al.* [2004]. The shortest *e*-folding times, that is, the conditions most prone to crescentic bar formation, occur for large wave height, long wave period, fine sediment and normal incidence. The shorter growth times for increasing wave height and decreasing grain size is reasonable if the starting point is at low intermediate beach conditions [*Wright and Short*, 1984; *Lippmann and Holman*, 1990]. However, at some point, the tendency should reverse since crescentic bars are commonly not present for highly dissipative beach conditions. The present model is unable to reproduce this stabilization. Comparison with the work of *Caballeria et al.* [2002], where this tendency was obtained, suggests that this is probably due to the different bed-slope sediment transport used by both models. More attention has to be paid in the future to the bed-slope terms in sediment transport formulations.

[63] The other mode describes the formation of short transverse bars (length about 10 m) with spacings of a few tens of meters. It is remarkable that their formation mechanism is not essentially linked to wave refraction as was the case for the long transverse bars for a planar beach in the work of *Caballeria et al.* [2002].

[64] Refraction favors significantly the secondary circulation cell along with the formation of mega cusps and confines the crescentic pattern and rip current cell on the bar. Wave phase perturbations increase the rip channel spacing and slow down its growth. In general, however, wave refraction does not influence substantially the initial formation of crescentic bars.

References

Aagaard, T. (1991), Multiple-bar morphodynamics and its relation to low-frequency edge waves, *J. Coastal Res.*, 7, 801–813.

Battjes, J. A. (1975), Modeling of turbulence in the surfzone, paper presented at Symposium on Modeling Techniques: Second Annual Symposium of the Waterways, Harbors, and Coastal Engineering Divisoin of ASCE, Am. Soc. of Civ. Eng., San Francisco, Calif.

Bowen, A. J., and D. L. Inman (1971), Edge waves and crescentic bars, *J. Geophys. Res.*, 76, 8662–8671.

Caballeria, M., G. Coco, A. Falqués, and D. A. Huntley (2002), Self-organization mechanisms for the formation of nearshore crescentic and transverse sand bars, *J. Fluid Mech.*, 465, 379–410.

Caballeria, M., D. Calvete, G. Coco, N. Dodd, and A. Falqués (2003), Formation and alongshore spacing of crescentic bars, paper presented at 3rd IAHR Symposium on River, Coastal and Estuarine Morphodynamics, Int. Assoc. for Hydraul. Res., Delft, Netherlands.

Calvete, D., and H. E. de Swart (2003), A nonlinear model study on the long-term behavior of shore face-connected sand ridges, *J. Geophys. Res.*, 108(C5), 3169, doi:10.1029/2001JC001091.

Calvete, D., N. Dodd, and A. Falqués (2003), Morphological development of nearshore bed forms, in *Coastal Engineering 2002*, vol. 3, edited by J. M. Smith, pp. 3321–3332, World Sci., River Edge, N. J.

Castelle, B. (2004), Modélisation de l'hydrodynamique sédimentaire au-dessus des barres sableuses soumises à l'action de la houle: application à la côte aquitaine, Ph.D. thesis, Univ. Bordeaux I, Talence, France.

Christensen, E., R. Deigaard, and J. Fredsoe (1994), Sea bed stability on a long straight coast, in *Coastal Engineering 1994*, vol. 4, edited by B. L. Edge, pp. 1865–1879, Am. Soc. of Civ. Eng., Reston, Va.

Coco, G., M. Caballeria, A. Falqués, and D. H. Huntley (2003), Crescentic bars and nearshore self-organization processes, in *Coastal Engineering 2002*, vol. 3, edited by J. M. Smith, pp. 3765–3777, World Sci., River Edge, N. J.

Damgaard, J., N. Dodd, L. Hall, and T. Chesher (2002), Morphodynamic modelling of rip channel growth, *Coastal Eng.*, 45, 199–221.

Deigaard, R. (1990), The formation of rip channels on barred coasts, *Tech. Rep. Prog. Rep. 72*, Inst. of Hydrodyn. and Hydraul. Eng. (ISVA), Lyngby, Denmark.

Deigaard, R., N. Drønen, J. Fredsoe, J. H. Jensen, and M. P. Jørgesen (1999), A morphological stability analysis for a long straight barred coast, *Coastal Eng.*, 36, 171–195.

Dodd, N., P. Blondeaux, D. Calvete, H. E. de Swart, A. Falqués, S. J. M. H. Hulscher, G. Różyński, and G. Vittori (2003), The use of stability methods in understanding the morphodynamical behavior of coastal systems, *J. Coastal Res.*, 19, 849–865.

Falqués, A., A. Montoto, and V. Iranzo (1996), Bed-flow instability of the longshore current, *Cont. Shelf Res.*, 16(15), 1927–1964.

Falqués, A., G. Coco, and D. A. Huntley (2000), A mechanism for the generation of wave-driven rhythmic patterns in the surf zone, *J. Geophys. Res.*, 105, 24,071–24,088.

Haller, M. C., R. A. Dalrymple, and I. A. Svendsen (2002), Experimental study of nearshore dynamics on a barred beach with rip channels, *J. Geophys. Res.*, 107(C6), 3061, doi:10.1029/2001JC000955.

Hino, M. (1974), Theory on formation of rip-current and cuspidal coast, in *Coastal Engineering 1974*, pp. 901–919, Am. Soc. of Civ. Eng., Reston, Va.

Holman, R. A., and A. J. Bowen (1982), Bars, bumps, and holes: Models for the generation of complex beach topography, *J. Geophys. Res.*, 87, 457–468.

Iranzo, V., and A. Falqués (1992), Some spectral methods for differential equations in unbounded domains, *Comput. Methods Appl. Mech. Eng.*, 98, 105–126.

Klein, M. D., H. M. Schuttelaars, and M. J. F. Stive (2003), Linear stability of a double-barred coast, in *Coastal Engineering 2002*, vol. 3, edited by J. M. Smith, pp. 3396–3408, World Sci., River Edge, N. J.

Lippmann, T. C., and R. A. Holman (1990), The spatial and temporal variability of sand bar morphology, *J. Geophys. Res.*, 95, 11,575–11,590.

Longuet-Higgins, M. S., and R. W. Stewart (1964), Radiation stresses in water waves: A physical discussion with applications, *Deep Sea Res.*, 11, 529–562.

Mei, C. C. (1989), *The Applied Dynamics of Ocean Surface Waves*, *Adv. Ser. Ocean Eng.*, vol. 1, World Sci., River Edge, N. J.

Niederoda, A. W., and W. F. Tanner (1970), Preliminary study on transverse bars, *Mar. Geol.*, 9, 41–62.

O'Reilly, W. C., and R. T. Guza (1993), A comparison of two spectral wave models in theSouthern California Bight, *Coastal Eng.*, 19, 263–282.

Reniers, A. J. H. M., J. A. Roelvink, and E. B. Thornton (2004), Morphodynamic modeling of an embayed beach under wave group forcing, *J. Geophys. Res.*, 109, C01030, doi:10.1029/2002JC001586.

Ribas, F., A. Falqués, and A. Montoto (2003), Nearshore oblique sand bars, *J. Geophys. Res.*, 108(C4), 3119, doi:10.1029/2001JC000985.

Soulsby, R. L. (1997), *Dynamics of Marine Sands*, Thomas Telford, London.

Thornton, E. B., and R. T. Guza (1983), Transformation of wave height distribution, *J. Geophys. Res.*, *88*, 5925–5938.

van Enckevort, I. M. J., B. G. Ruessink, G. Coco, K. Suzuki, I. L. Turner, N. G. Plant, and R. A. Holman (2004), Observations of nearshore crescentic sandbars, *J. Geophys. Res.*, *109*, C06028, doi:10.1029/2003JC002214.

Vittori, G., H. E. de Swart, and P. Blondeaux (1999), Crescentic bedforms in the nearshore region, *J. Fluid Mech.*, *381*, 271–303.

Wright, L. D., and A. D. Short (1984), Morphodynamic variability of surf zones and beaches: A synthesis, *Mar. Geol.*, *56*, 93–118.

Yu, J., and D. N. Slinn (2003), Effects of wave-current interaction on rip currents, *J. Geophys. Res.*, *108*(C3), 3088, doi:10.1029/2001JC001105.

————————————

D. Calvete and A. Falqués, Departament de Física Aplicada, Universitat Politécnica de Catalunya, Campus Nord - Modùl B4, 08034 Barcelona, Spain. (calvete@fa.upc.es; falques@fa.upc.es)

N. Dodd and S. M. van Leeuwen, School of Civil Engineering, University of Nottingham, University Park, Nottingham, NG7 2RD, UK. (nick.dodd@nottingham.ac.uk; sonja.vanleeuwen@nottingham.ac.uk)